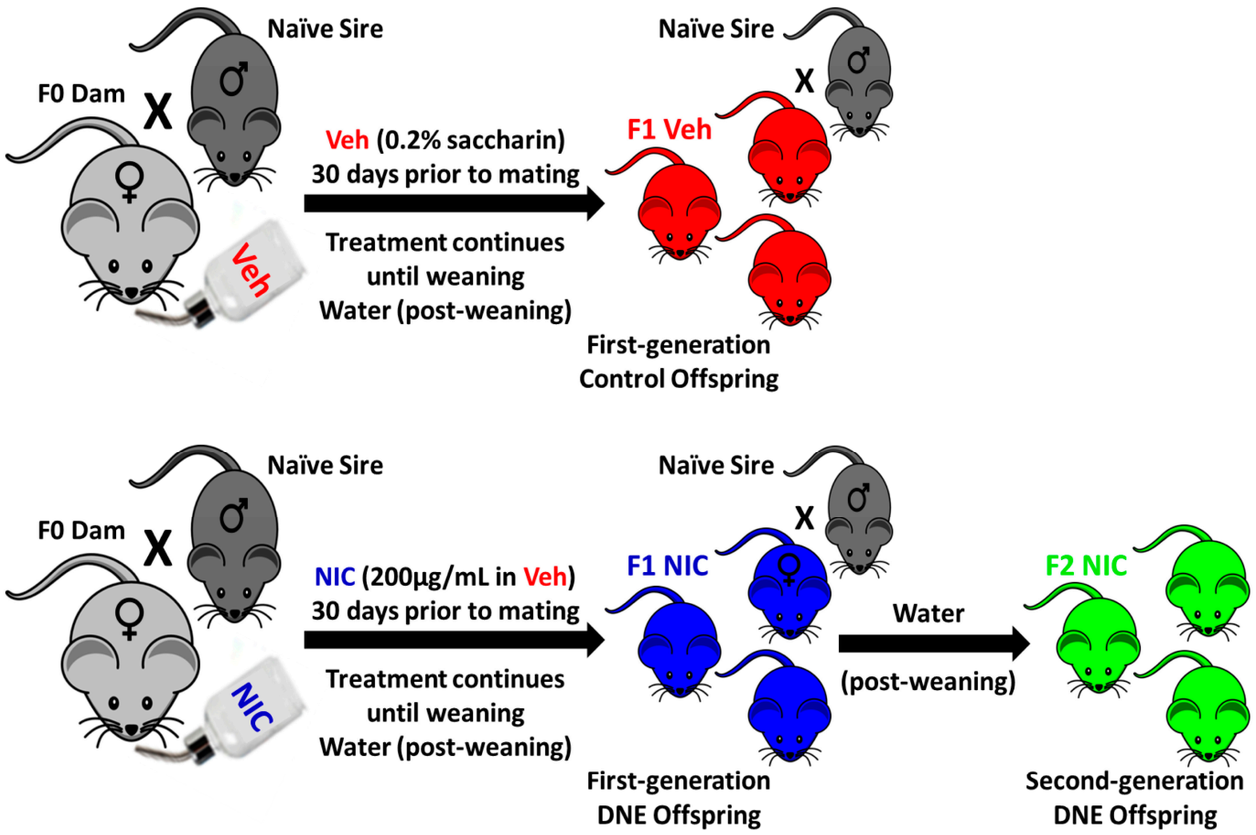


Phenotypes of Interest:	First-generation DNE Progeny:	Second-generation DNE Progeny:
• Active phase hyperactivity	✓	✓
• Inactive phase hyperactivity	✓	✓
• Hyperactivity in a novel context	✓	✓
• Increased risk-taking	✓	✓
• Increased NIC intake/preference	✓	✓
• Aberrant rhythmicity of activity	✓	✓
• Therapeutic effects of MPH + NIC	✓	✓
• Altered nAChR binding/function	✓	✓
• Impaired DAT function	✓	✓
• Impaired proBDNF proteolysis	✓	✓
• GR hypoactivity + CORT deficits	✓	✓
• 5-mC/DNMT3A/MeCP2 deficits	✓	✓
• HDAC2 downregulation	✓	✓

Figure S1. *Procedural Schematic for breeding of DNE progeny and compilation of key findings from our prior studies utilizing the same DNE mouse model paradigm.* (Top) Female breeders (F0 Dams) were exposed to 0.2% saccharin (Vehicle, Veh) or 0.2% saccharin with 200µg/mL nicotine (DNE) in drinking water for 30 days prior to mating with drug-naïve males (naïve sires). Vehicle or nicotine treatment of breeders continued until weaning of offspring at PND 21, after which water was provided as the sole fluid source for all offspring. Randomly selected female F1 DNE offspring were subsequently mated with drug-naïve male sires to obtain F2 DNE offspring. (Bottom) Comprehensive synopsis of NDD-like phenotypes that we have previously reported in DNE offspring and grandoffspring. The present study endeavored to build upon our prior research by conducting a novel characterization of the multigenerational impacts of DNE on the translatome of D1 MSNs. PND, post-natal day; Veh, 0.2% aqueous saccharin; NIC, 200 µg/mL nicotine in 0.2% saccharin; F1 Veh, first-generation developmental vehicle-exposed offspring; F1 NIC, first-generation DNE offspring; F2 NIC, second-generation DNE offspring.

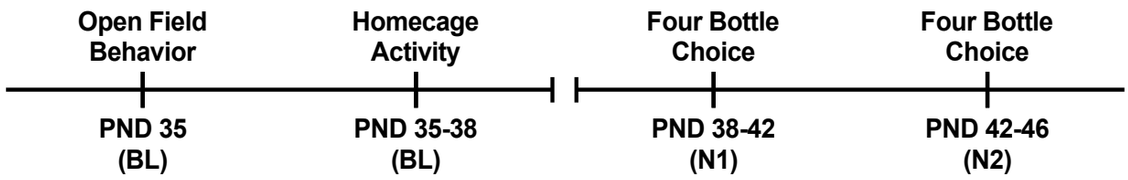


Figure S2. *Procedural timeline for baseline behavioral characterization*. For baseline (BL) behavioral characterization, all mice were first subjected to open field testing (OFT) on PND 35 and were then immediately transferred to a modified homecage (HC) to undergo activity monitoring for three consecutive days. Four-bottle choice testing (FBCT) was then conducted within the same modified home cages to assess voluntary nicotine consumption and preference. For OFT, locomotor activity in a novel environment and risk-taking behaviors were evaluated as described in our previous studies [54, 109]. Briefly, mice were subjected to 15-minute open field trials in a 40x40cm opaque plexiglass arena at baseline. Activity Monitor (Med Associates Inc., Fairfax, VT) was used for data collection and analysis. Total distance moved in the open field was evaluated as the outcome measure for locomotor activity in a novel environment. Risk-taking behavior was assessed by measuring the percent of total distance moved in the center 10x10cm area of the open field arena. Percent of total distance moved was used rather than center time in order to control for individual differences in OFA activity. For HC activity monitoring, locomotor activity of singly housed mice was continuously recorded during a three-day baseline period using cagetop-mounted infrared motion sensors and VitalView Data Acquisition software (Starr Life Sciences Corporation, Oakmont, PA). Activity counts per day (separated by active and inactive phase) served as the dependent variable for passive HC activity monitoring. In addition to summary measures of activity, rhythmometric analyses were performed to probe for potential ADHD-like alterations in the HC activity rhythms of DNE mice (see Fig. S3 below for more details on activity rhythm analyses). For FBCT, drinking solutions were supplied in Pyrex test tubes (9820, 18mm x 150 mm, Fisher Scientific) fitted with rubber septa (Suba-Seal septa 29; Sigma Aldrich) containing a standard 6.5mm stainless steel sipper tube. Tubes containing water, 25 µg/mL nicotine, 50 µg/mL nicotine, and 100 µg/mL nicotine were placed in four equidistant holes fashioned in one side of conventional polycarbonate homecages, and food was placed directly in the cage bottom. FBCT was conducted over two continuous four-day intervals (N1, N2). Bottles were weighed before and after N1 and N2 and were rotated daily to eliminate confounding due to position bias. Daily nicotine consumption (mg/kg/day) was calculated as the outcome measure for voluntary nicotine intake, and preference ratios (volume consumed from each bottle divided by the total daily fluid consumed) were calculated as the outcome measure for nicotine preference at each concentration tested.

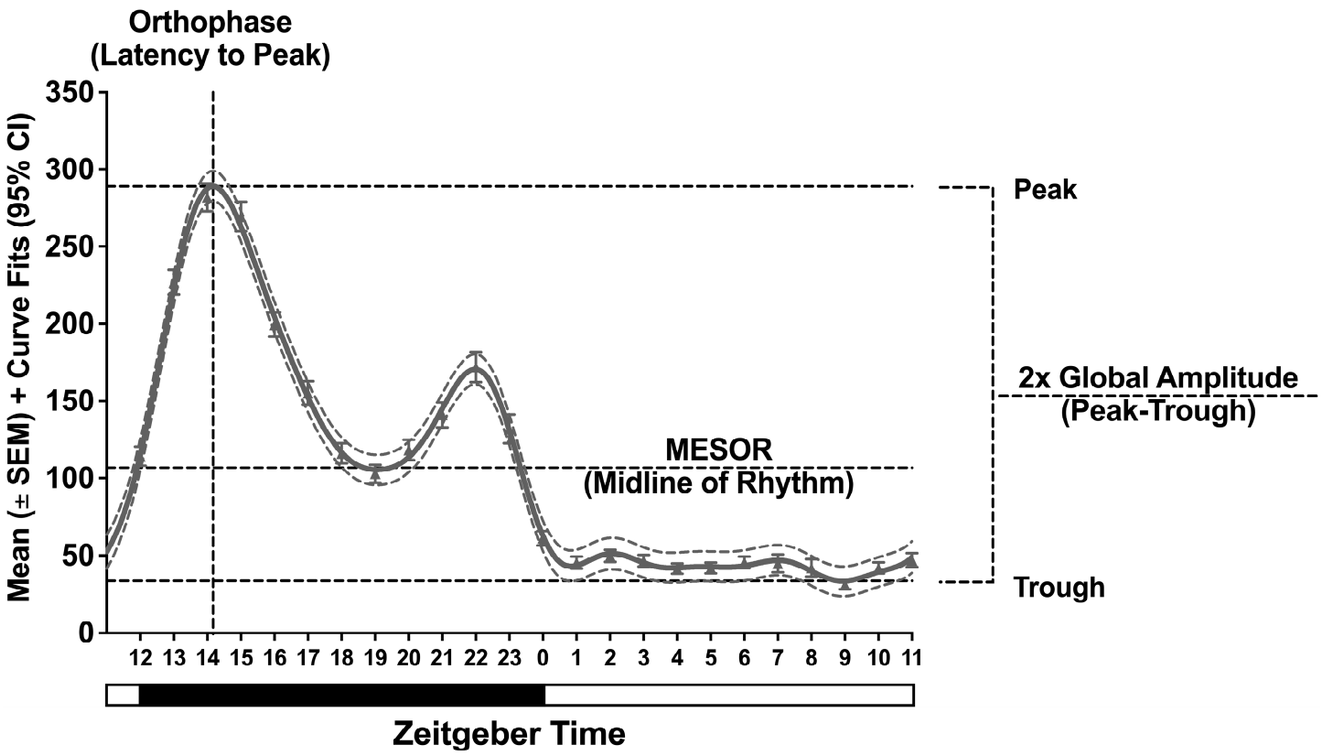


Figure S3. *Schematic depicting the global (composite) parameters used to characterize HC activity rhythms.* Diagram depicting the global parameters of rhythm superimposed on a representative curve fit of HC activity. Rhythmicity of home cage locomotor activity was assessed using a multi-harmonic regression model expressing the fundamental period and multiple discrete harmonics. To identify the fundamental period and its discrete harmonics, raw activity data were collapsed into hourly bins for each group and experimental phase, and frequency decomposition was performed via harmonic regression at Fourier frequencies. The zero-amplitude F-test was next used to test the null hypothesis of zero amplitude for the fundamental period and each harmonic identified by frequency decomposition. The fundamental period and each of its harmonics with significant non-zero amplitude were then incorporated stepwise into a preliminary multiharmonic cosinor model that was used to fit the raw activity data for each group at each experimental phase. The extra sum of squares F-test was applied in concert to select for only those components which explained a significantly greater proportion of the total variance (percentage of rhythm) when included in the model, based on comparison to a nested model lacking that component with the null hypothesis that the simpler, nested model is correct. Applying this approach for each group at each experimental stage, we identified the simplest model necessary to adequately fit the data for each group as measured by the Replicates Test (F-test for lack of fit). In addition to the fundamental near-24h period, the zero-amplitude test identified multiple harmonic periods with significant non-zero amplitude, and the exact sum of squares F-test confirmed that each of these periods explained a significant proportion of the total variance (percentage rhythm) for each group at each experimental stage. Regression diagnostic measures including the replicates test for lack of fit and composite percentage rhythm calculations confirmed the adequacy of each model used. The multi-harmonic regression models generated by this approach were used to analyze hourly-binned raw HC activity data separately for each mouse at each experimental stage, and the Runs Test was conducted to verify goodness of fit of the models used for each subject at each experimental stage. These analyses yielded individual estimates for parameters of rhythm including the global MESOR (midline of rhythm) and the amplitude (peak - MESOR) and acrophase (time at peak) of the fundamental period and each harmonic expressed in the models. To characterize the composite activity rhythms of each mouse, estimates of the global amplitude (composite peak - trough) and orthophase (time at composite peak) were interpolated from each model. Composite parameter estimates obtained for each mouse were collapsed by group and experimental stage and compared both within and between groups using two-way repeated measures ANOVA. The general framework for the multiharmonic regression models was defined by the following equation:

$$Y(t) = M + \sum jAj\cos(2\pi/\tau j + \phi j) + e(t),\ j = 1, 2, 3, 4, 5, 6$$

Where Y = activity counts; t = time; M = MESOR (ymid); A = amplitude (ymax - ymid); τ = period (cycle duration, in hours); ϕ = acrophase (value of t at ymax); and e(t) = error term

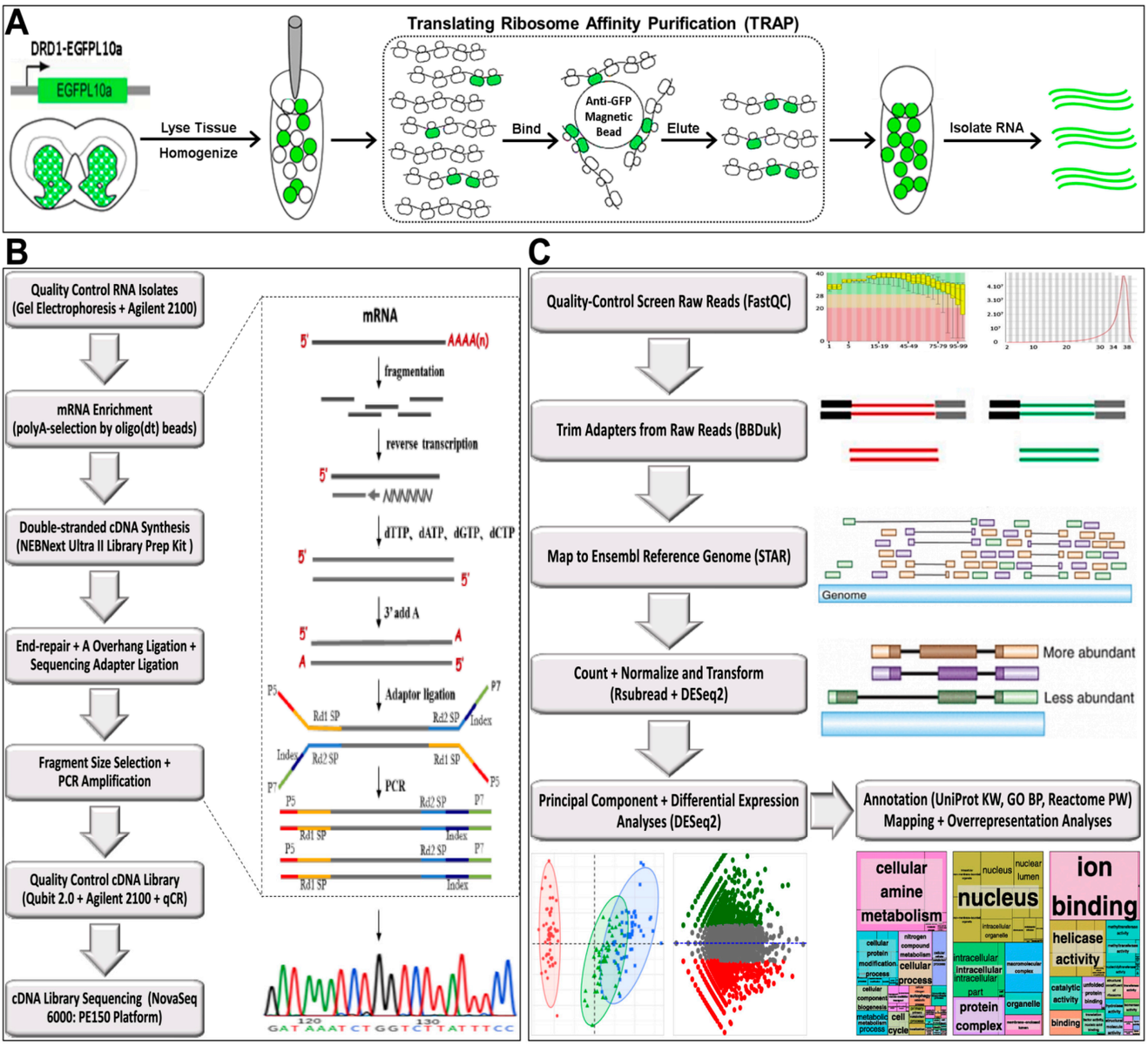


Figure S4. *Workflow visualizations for translating ribosome affinity purification, RNA sequencing, and bioinformatic and differential translatomic analyses.* **(A)** Workflow for RNA isolation from DRD1-expressing striatal cells of DRD1-EGFPL10a mice via translating ribosome affinity purification (TRAP). Striatal tissues from DRD1-EGFP/Rpl10a mice were homogenized and EGFP-tagged polysome-mRNA complexes from DRD1-expressing striatal cells were then immunoprecipitated from tissue homogenates using anti-EGFP-conjugated Dynabeads. Immunoprecipitated Dynabead-polysome complexes were eluted using a magnetic tube rack and RNA were isolated from polysomes using a Qiagen RNeasy Kit. **(B)** Workflow for RNA sequencing experiments encompassing mRNA enrichment, cDNA library preparation and quality control screening, and high-throughput sequencing steps. Qualified RNA isolates were enriched for mRNA (and depleted of rRNA) via polyA-selection using oligo(dt) beads. Double stranded cDNA libraries were then synthesized by reverse transcription of fragmented mRNA followed by second cDNA strand synthesis. Terminal (end) repair, A-overhang ligation, and sequencing adapter ligation were conducted, after which cDNA libraries were finished by size-selection (150bp) and PCR amplification. For quantification and quality control screening of finished cDNA libraries, a Qubit 2.0 was utilized to determine preliminary cDNA concentrations, an Agilent 2100 Bioanalyzer was used to evaluate insert sizes, and qPCR was conducted to precisely quantify effective cDNA library concentrations. Qualified cDNA libraries were then paired-end sequenced using an Illumina NovaSEQ6000, yielding approximately 20 million paired-end 150bp reads per sample (approximately 40 million actual 150bp reads). **(C)** Workflow for bioinformatic (top-to-bottom) and differential translatomic (left-to-right) analyses. The raw cDNA library sequencing data obtained were transformed to sequenced reads via base calling and recorded in FASTQ files alongside sequencing quality measurements. Sequencing data were quality-controlled via FastQC, trimmed of adapters using BBDuk, and aligned to the Ensembl mouse genome via STAR. Aligned reads were counted via Rsubread. Read count data were normalized and regularized log-transformed via DESeq2. Principal component and differential translation analyses were conducted using DESeq2. Functional (UniProt Keyword, UniProt KW), ontological (G.O. Biological Process, GO BP), and pathway (Reactome Pathway, Reactome PW) annotation mapping and overrepresentation analyses were conducted via STRING, PANTHER, and STRING, respectively.

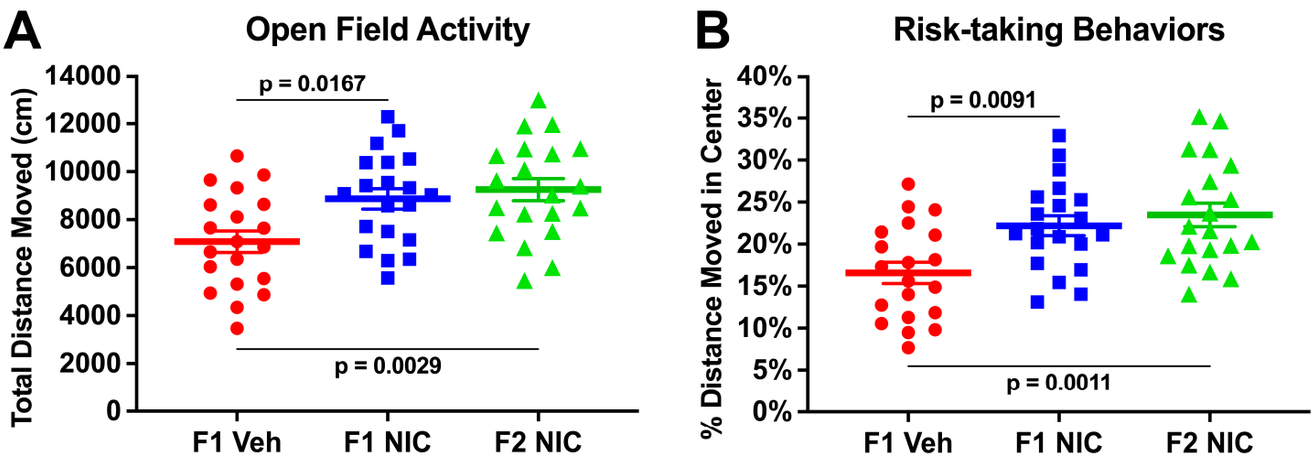


Figure S5. *DNE elicits multigenerational hyperactivity and risk-taking behaviors in adolescent DRD1-EGFP/Rpl10a mice.* Baseline data for open field behavior in adolescent C57BL/6J mice (primary cohort). Datasets for total distance moved and percent distance moved in the center of the open field were analyzed by one-way ANOVA with the between-subjects factor group. One-way ANOVA revealed a main effect of group ($F_{2,57}$ = 6.82; P=0.0022) for total distance moved in the open field. One-way ANOVA also revealed a main effect of group ($F_{2,57}$ = 8.07; P=0.00082) for percent distance moved in the center of the open field. **(A)** *Total distance moved (cm) in a 15-minute open field (open field) trial*. F1 NIC and F2 NIC mice moved a greater total distance in the open field compared to F1 Veh. **(B)** *Percent distance moved in the center of the open field*. F1 NIC and F2 NIC mice moved a greater percent of total distance in the center of the open field compared to F1 Veh. For all baseline behavioral datasets, n_{F1Veh}=20, n_{F1NIC}=20, and n_{F2NIC}=20. Adjusted p-values for all pairwise comparisons are displayed within the corresponding figure panels. All data are mean ± S.E.M.

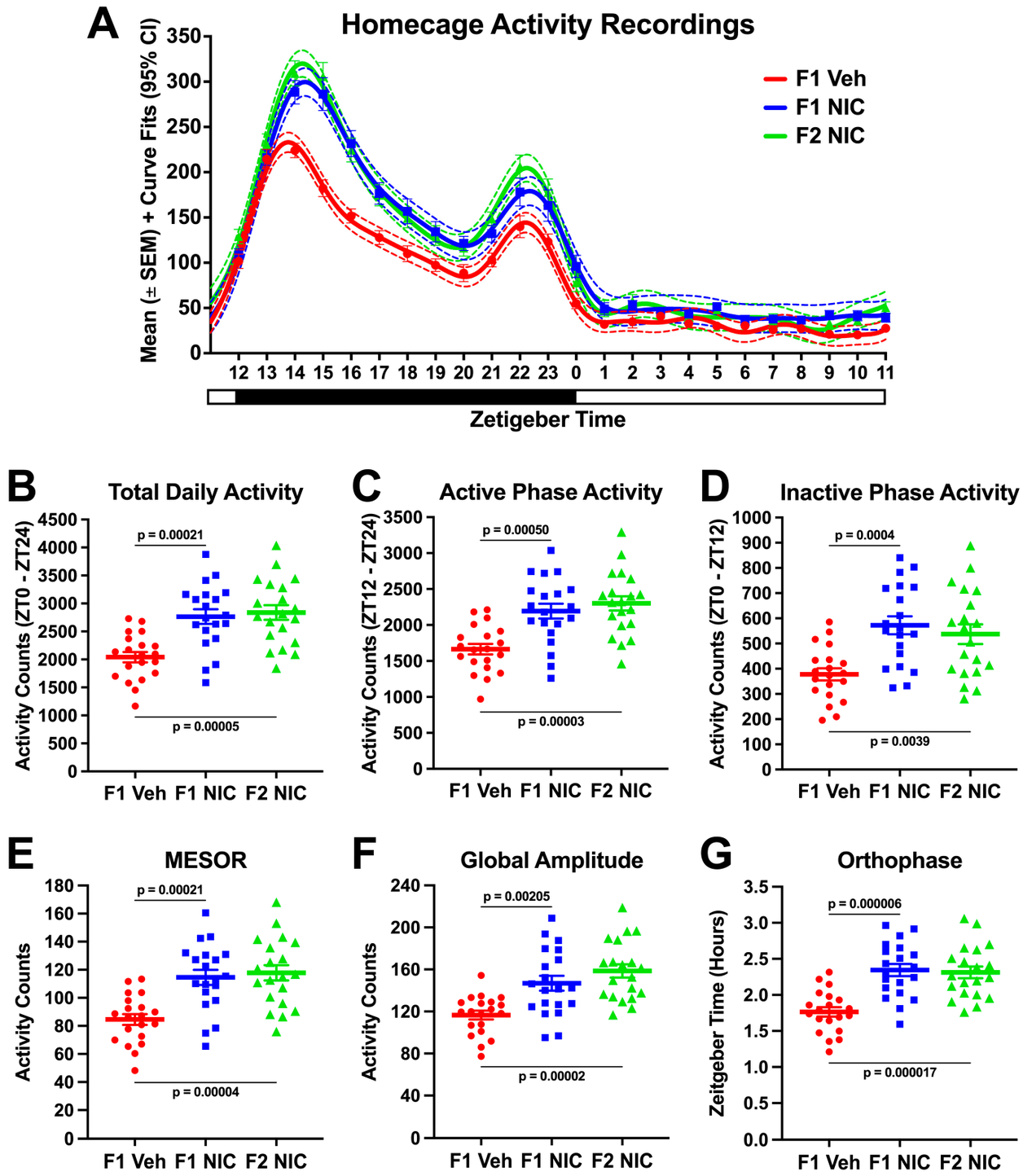


Figure S6. *DNE elicits multigenerational homecage hyperactivity and aberrant rhythmicity of homecage activity at baseline in adolescent DRD1-EGFP/Rpl10a mice.* **(A)** Representative plots of average daily homecage activity over a three-day baseline period collapsed into hourly bins (floating points depicting mean ± S.E.M) with superimposed multi-harmonic regression curve fits (mean ± 95% CI bands). Summary home cage locomotor activity data (B, C, and D) and activity rhythm parameter estimates (E, F, and G) were analyzed by mixed ANOVA with the between-subjects factor group and the within-subjects factor measure (total daily, active phase, and inactive phase or MESOR, global amplitude, and orthophase, respectively). Mixed ANOVA detected main effects of group ($F_{2,57}$ = 13.63; P=0.000015) and measure ($F_{1.144,65.21}$ = 1362; P<0.000000000000001) and a significant group x measure interaction ($F_{2.288,65.21}$ = 12.37; P=0.000012) for summary home cage locomotor activity. Mixed ANOVA detected main effects of group ($F_{2,57}$ = 15.25; P=0.0000049) and measure ($F_{1.651,94.08}$ = 1231; P<0.000000000000001) and a significant group x bottle interaction ($F_{3.301,94.08}$ = 10.59; P=0.0000021) for activity rhythm parameter estimates. **(B)** *Total daily homecage activity.* F1 NIC and F2 NIC mice exhibited increased total daily activity compared to F1 Veh at baseline. **(C)** *Active phase homecage activity*. F1 NIC and F2 NIC mice were more active than F1 Veh during the active phase at baseline. **(D)** *Inactive phase homecage activity*. F1 NIC and F2 NIC mice were more active than F1 Veh during the inactive phase at baseline **(E)** *MESOR estimates*. F1 NIC and F2 NIC mice had increased MESOR estimates at baseline compared to F1 Veh). **(F)** *Global amplitude estimates.* F1 NIC and F2 NIC mice had increased global amplitude estimates at baseline compared to F1 Veh. **(G)** *Orthophase estimates.* F1 NIC and F2 NIC mice had delayed orthophase estimates at baseline compared to F1 Veh. For all behavioral datasets, n_{F1Veh}=20, n_{F1NIC}=20, and n_{F2NIC}=20. Adjusted p-values for all pairwise comparisons are displayed within the corresponding figure panels. All data are mean ± S.E.M unless otherwise noted.

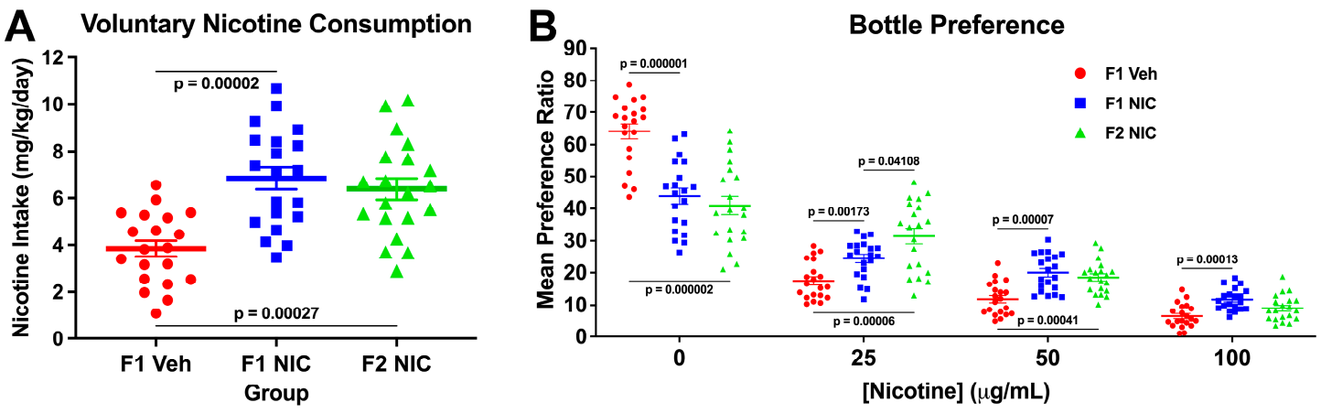


Figure S7. *DNE elicits multigenerational enhancement of voluntary nicotine intake and preference in adolescent DRD1-EGFP/Rpl10a mice.* Data for voluntary nicotine intake in the four-bottle choice test were analyzed by one-way ANOVA with the between-subjects factor group. Data for bottle preference in the four-bottle choice test were analyzed by mixed ANOVA with the between-subjects factor group and the within-subjects factor bottle (preference for water, preference for 25μg/mL nicotine, preference for 50μg/mL nicotine, or preference for 100μg/mL nicotine). One-way ANOVA revealed a main effect of group ($F_{2,57}$ = 14.3; P=0.0000092) for FBCT voluntary nicotine intake. Mixed ANOVA detected main effects of group ($F_{2,57}$ = 5.64; P=0.0058) and bottle ($F_{1.526,86.97}$ = 238.8; P<0.000000000000001) and a significant group x bottle interaction ($F_{3.052,86.97}$ = 20.0; P=0.00000000048) for FBCT bottle preference. **(A)** *Voluntary nicotine intake (mg/kg/day) in the four-bottle choice test.* F1 NIC and F2 NIC mice consume more nicotine than F1 Veh, and F1 NIC mice consume more nicotine than F2 NIC. **(B)** *Nicotine preference ratios for the four-bottle choice test*. F2 NIC mice consume more 25μg/mL nicotine than F1 Veh and F1 NIC. F1 NIC and F2 NIC mice consume more 50μg/mL nicotine than F1 Veh. F1 NIC mice consume more 100μg/mL nicotine than F1 Veh and F2 NIC. F1 Veh mice consume more plain water (0μg/mL) than F1 NIC and F2 NIC mice, and F2 NIC mice consume more plain water than F1 NIC. For all baseline behavioral datasets, n_{F1Veh}=20, n_{F1NIC}=20, and n_{F2NIC}=20. Adjusted p-values for all pairwise comparisons are displayed within the corresponding figure panels. All data are mean ± S.E.M.

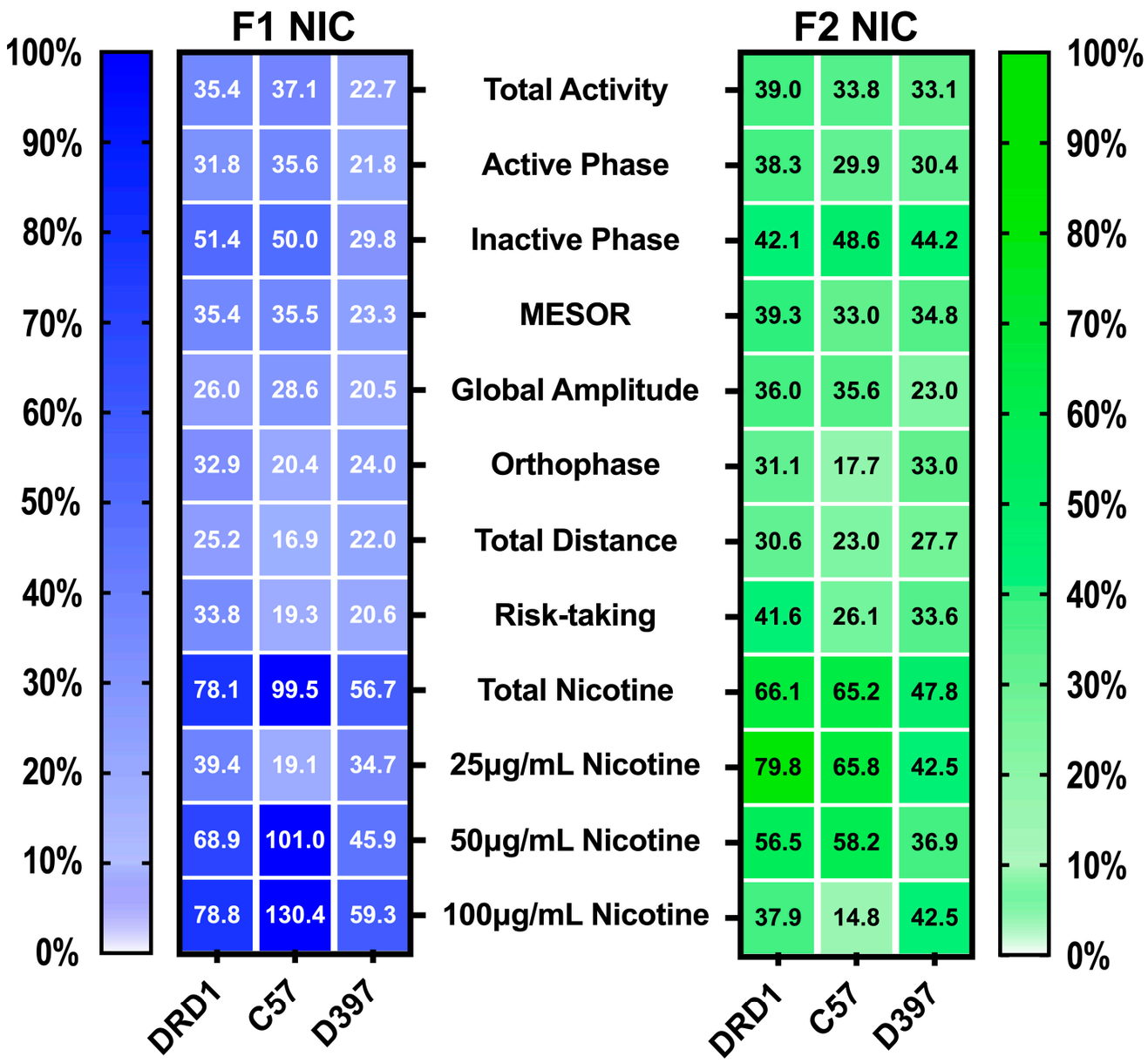


Figure S8. *Comparison of baseline behavioral phenotypes among C57BL/6J, D397, and DRD1-EGFP/Rpl10a DNE offspring and grandoffspring.* Single-gradient heatmaps depicting the percentage increases relative to F1 Veh control mice in each outcome measure (vertical axis) and group (horizontal axis) for C57BL/6J (left) and D397 (middle) DNE offspring and grandoffspring from our preceding studies and for DRD1-EGFP/Rpl10a (right) DNE offspring and grandoffspring from the present study. A percentage increase of zero indicates no difference relative to F1 Veh control mice, whereas a percentage increase of 100% indicates a two-fold increase relative to F1 Veh control mice. The relative color saturation of each heatmap cell is proportional to the percentage increase relative to F1 Veh for the corresponding outcome measure. C57, C57BL/6J cohort; D397, D397 cohort; DRD1, DRD1-EGFP/Rpl10a cohort.

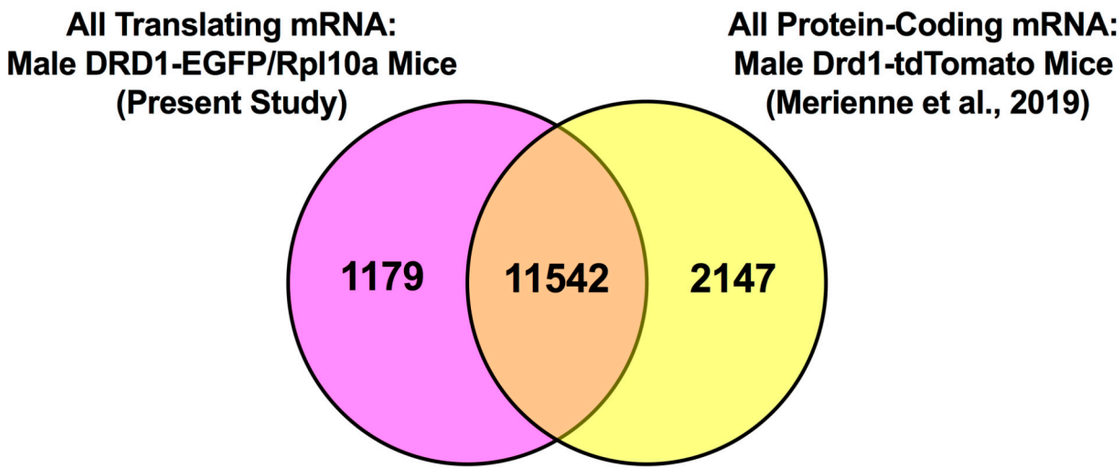


Figure S9. *Comparison of the consensus translatome for DRD1-expressing striatal cells of DRD1-EGFP/Rpl10a mice from the present study to a consensus protein-coding transcriptome for DRD1-expressing striatal cells of male Drd1-tdTomato mice.* Venn diagram quantitatively comparing the consensus translatome of DRD1-expressing striatal cells of DRD1-EGFP/Rpl10a mice to the consensus protein-coding transcriptome for DRD1-expressing striatal cells of male Drd1-tdTomato mice. 11,542 elements intersected (overlapped) between while 1179 and 2147 elements were distinct to the consensus translatome for DRD1-expressing striatal cells of DRD1-EGFP/Rpl10a mice and the consensus protein-coding transcriptome for DRD1-expressing striatal cells of male Drd1-tdTomato mice, respectively, yielding a Jaccard similarity index of 0.7763.

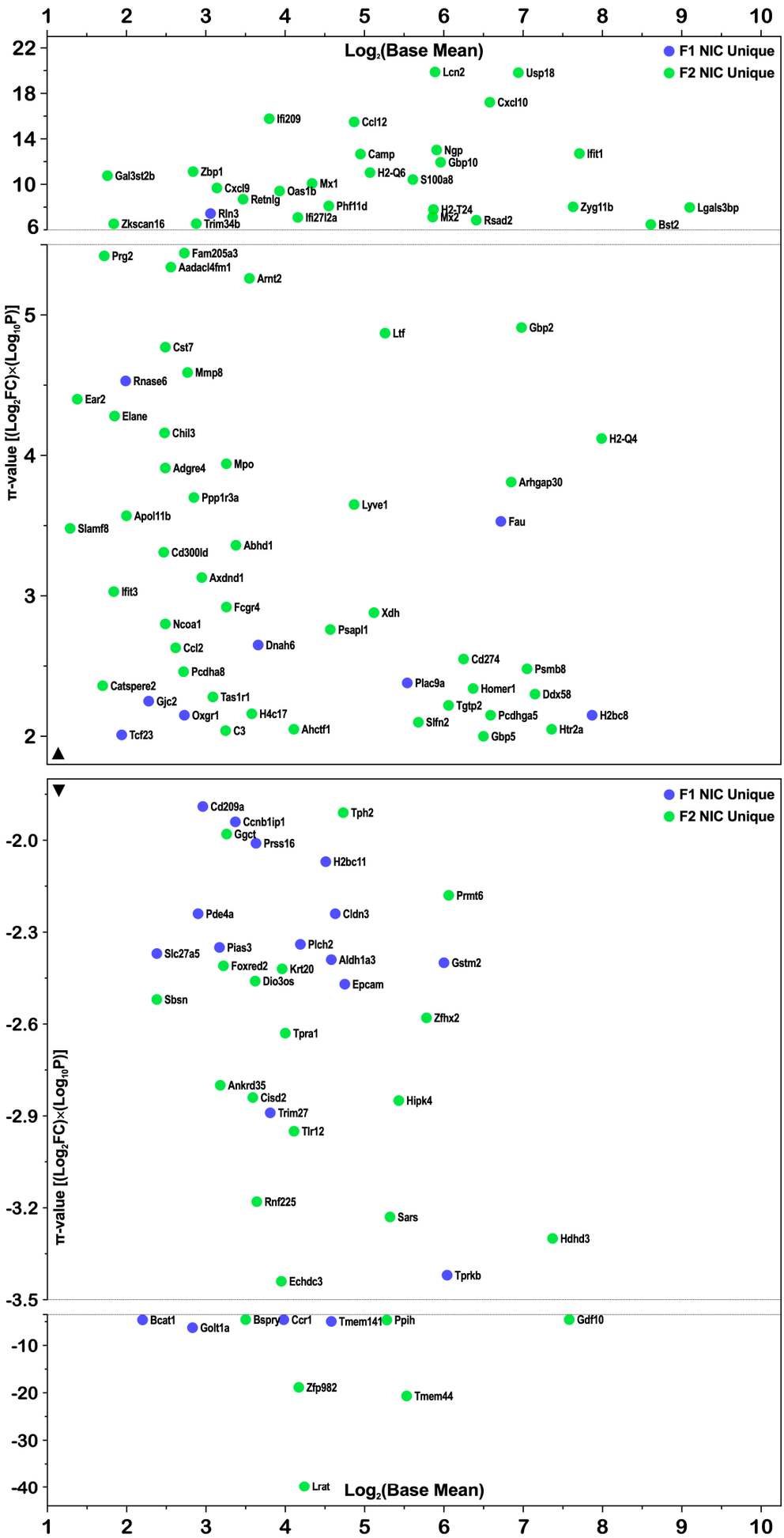


Figure S10. *Comparative stratification of DEGs uniquely detected in F1 NIC or F2 NIC mice.* For all unique DEGs, π-values (π = $Log_2FC^*(Log_{10}P)$) were calculated to provide a single composite metric that integrates both fold change (magnitude or biological significance) and p-value (statistical significance). Positive and negative π-value thresholds were applied to stratify unique DEGs into subsets that fall within or without the range of $-2 < \pi < 2$. DEGs for which $\pi < -2$ or $\pi > +2$ have stronger potential to be robust mediators of DNE impacts that may not undergo intergenerational transmission at the level of differential gene expression. π-values for unique DEGs with $\pi < -2$ (▼) or $\pi > +2$ (▲) and corresponding Log_2(base mean) values are plotted on the vertical and horizontal axes, respectively. Discontinuously scaling of the vertical axis enabled visualization of more DEGs.

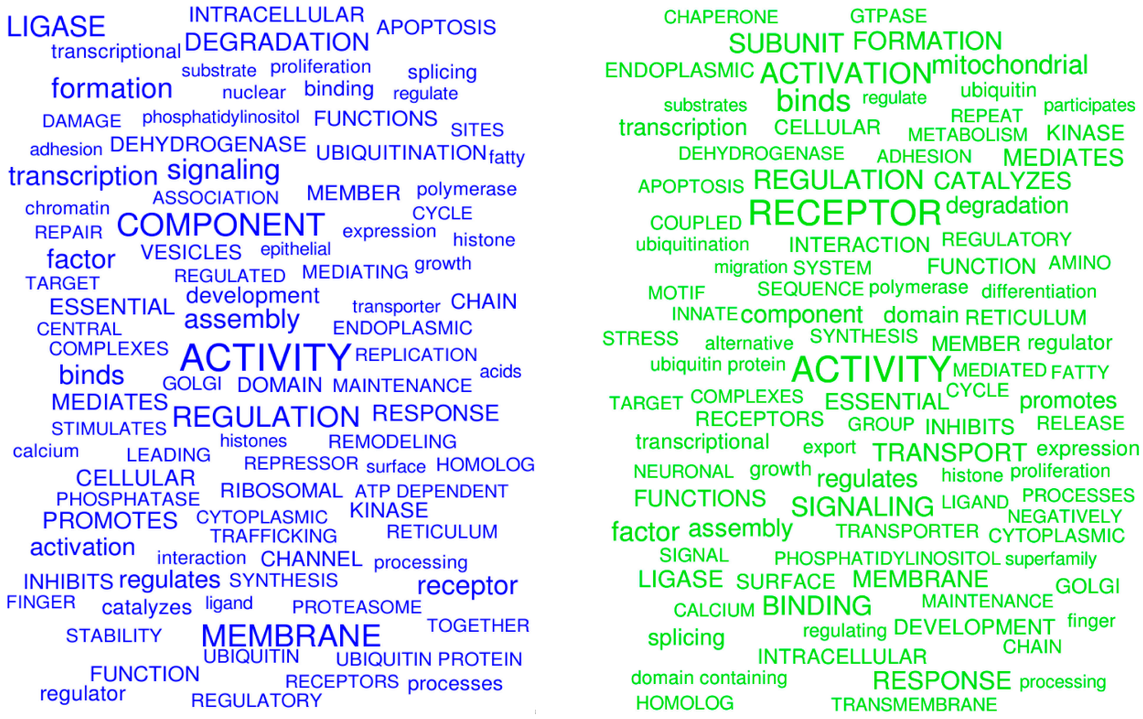


Figure S11. *Word clouds generated by word frequency analyses of STRING protein annotations retrieved for enriched and depleted DEGs uniquely detected in F1 NIC or F2 NIC mice.* The word clouds generated for this study attribute broad biological themes to unique DEGs by scaling font size with absolute word frequencies assimilated from DEG-encoded STRING protein annotations. Absolute word frequency is proportional to font size (larger fonts for higher frequencies). For F1 NIC (blue word cloud, left) and F2 NIC (green word cloud, right) mice, words mapped to unique enriched DEGs appear ‘UPPERCASE’, and words mapped to unique depleted DEGs appear ‘lowercase’.